

Assessing the robustness of spatial pattern sequences in models of dryland vegetation

Karna Gowda¹, Yuxin Chen¹, Sarah Iams¹, and Mary Silber^{*1,2}

¹Department of Engineering Sciences and Applied Mathematics, Northwestern University, Evanston, IL 60208, USA

²Northwestern Institute on Complex Systems, Northwestern University, Evanston, IL 60208, USA

Abstract

A particular sequence of patterns, “gaps \rightarrow labyrinth \rightarrow spots”, occurs with decreasing precipitation in previously reported numerical simulations of PDE dryland vegetation models. This has led to the suggestion that this sequence of patterns can serve as an early indicator of desertification in some ecosystems. Since a range of parameter values and functional formulations are plausible in the vegetation models, it is important to investigate whether the pattern sequence prediction is robust to model variation. Using bifurcation theoretic analyses and numerical simulations, we find that amplitude equation coefficients can be used to assess where the sequence occurs in the parameter space of a widely studied model. This can be used to establish the standard sequence as a robust prediction of the model, and perhaps a more general class of models.

1 Introduction

Many studies of spatially periodic patterns in models of dryland vegetation focus on patterns as potential indicators of ecosystem vitality [1–13]. In particular, flat-terrain patterned states in several models have been shown in simulations to evolve through a sequence of morphologies, “gaps \rightarrow labyrinth \rightarrow spots” (Figure 1), as ecosystem aridity increases [1, 4, 14, 15]. This sequence precedes the collapse of vegetation in the models, which has led to the suggestion that real ecosystems may evolve through this predictable sequence of patterns en route to desertification [16, 17]. In this way, vegetation patterns may serve as early-warning signs of critical ecosystem transitions. The pattern sequence prediction emerges from a modelling framework comprising a number of different ecological hypotheses, functional formulations and definitions of plausible parameter sets. It is therefore important to investigate whether the prediction is robust within this framework. It is encouraging that multiple models can produce the pattern sequence “gaps \rightarrow labyrinth \rightarrow spots” (the standard sequence), but little work has been done to assess whether the sequence occurs in any model under variations of the parameter values, which may vary significantly between ecosystems. In this paper, we ask whether easily calculable quantities, derived from bifurcation theoretic analysis of pattern-forming instabilities, can be used to predict where the standard sequence occurs in a model’s parameter space. To do this, we analyse and simulate the widely studied model by Rietkerk *et al.* [14] across a broad range of parameter values.

The standard sequence, “gaps \rightarrow labyrinth \rightarrow spots”, is observed in a suite of partial differential equation

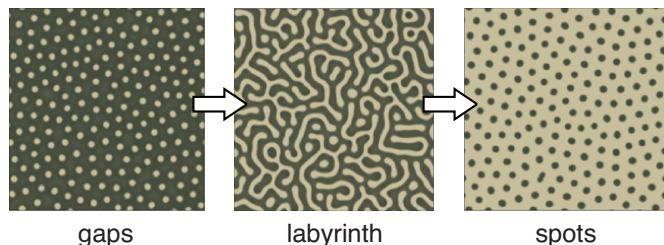


Figure 1: Example of the standard “gaps \rightarrow labyrinth \rightarrow spots” sequence in the vegetation model by Rietkerk *et al.* [14]. Qualitatively different patterns occur at successively smaller values of a precipitation parameter. Simulations are generated using the parameter set given by Zelnik *et al.* [11], which is listed in Table 2. Darker shading denotes higher levels of vegetation biomass.

(PDE) models that describe the community-scale dynamics of dryland vegetation over flat terrain [1, 4, 14, 15]. These models all invoke the Turing mechanism [18] for the formation of patterns from uniform vegetation. Observations of the standard sequence as a model prediction come primarily from numerical simulations [1, 4, 14], which show gap, labyrinth, and spot patterns occurring at successively lower values of a precipitation parameter (Figure 1). A study by LeJeune *et al.* [15] used bifurcation analysis to demonstrate analytically that this sequence occurs in a tractable 1-field model for a particular parameter set. The apparent agreement between these observations, which come from different model formulations, provides some support for the standard sequence as a robust prediction of this suite of models.

Empirical support for this sequence comes chiefly from

two studies of remotely-sensed imagery. A 2006 study by Barbier *et al.* [19] used imagery over southwest Niger to demonstrate that gap patterns emerged from uniform vegetation over a period of time coinciding with a prolonged Sahelian drought. This result is consistent with model observations of gap patterns occurring near the onset of pattern formation. A 2011 study by Deblauwe *et al.* [20] classified pattern morphologies in imagery over Sudan and found that different morphologies vary over spatial precipitation gradients in accordance with the standard sequence prediction. Gaps tended to occur in areas with relatively high mean annual precipitation, spots occurred in areas with relatively low precipitation, and labyrinths occurred in between. Pattern dynamics were also assessed using three sets of images taken over a 35-year span. Gaps in some areas were shown to transition to labyrinths over a period of time again coinciding with a sustained regional drought. Labyrinths transitioned to spots in different areas over the same period of time. Though neither of these studies show the standard sequence preceding the collapse of vegetation, they demonstrate consistency between model predictions and empirical observations.

Since these empirical studies focus on two Sub-Saharan regions, they are statements about particular ecosystems, which are subject to particular environmental and ecological parameters. It is unknown how other periodically-patterned flat-terrain ecosystems behave in response to changes in aridity. It is also unknown whether the suite of dryland vegetation models predicts the standard sequence to occur under most circumstances, since the numerical simulations underlying the standard sequence model observations were generated using a small number of parameter sets. The parameter sets appropriate for different ecosystems can differ significantly. For instance, the model for banded vegetation patterns on slopes by Klausmeier [21] distinguishes between shrublands and grasslands, using plant mortality parameters that differ by an order of magnitude for these different plant types¹. Little work has been done to systematically assess the sensitivity of the standard sequence prediction to model parameters. Such an assessment is important to understanding under what circumstances the sequence is predicted to be an early-warning sign.

We ask whether the standard sequence can be identified in a model using quantities calculated via bifurcation analysis. Gowda *et al.* [5] demonstrate that, in certain limits of model parameter values, pattern sequences can be studied analytically using bifurcation theory. This analysis shows that a particular nonlinear coefficient of the bifurcation problem affects the stability of weakly nonlinear patterns. If this coefficient changes its sign from negative to positive as a precipitation parameter is decreased in value, an analog of the standard sequence occurs in certain cases. Otherwise, alternative sequences,

such as one consisting only of spot patterns, can occur. Based on a preliminary model investigation, Gowda *et al.* [5] speculate that this coefficient also encodes information about pattern sequences that occur in more fully nonlinear cases. Here, we address this question systematically in the model by Rietkerk *et al.* [14] using numerical simulations across a broad range of parameter values.

If coefficients from bifurcation analysis can be used to identify the standard sequence, then they can be used to explore a model's parameter space more efficiently than by direct numerical simulation. This is important for analysing 3-field models, such as the models Rietkerk *et al.* [14] and Gilad *et al.* [11, 22], which depend on a large number of non-dimensional parameters. Since the coefficients are computed analytically, they can also be used to understand what model formulations and constraints lead to the standard sequence prediction. This analysis could shed light on the relative importance of different ecological processes to determining whether the standard sequence appears, which is another step towards a systematic understanding of when the sequence can serve as an early-warning sign.

2 Background

2.1 Model by Rietkerk *et al.* (2002)

We study the PDE vegetation model by Rietkerk *et al.* [14] (R02), which consists of three fields: plant biomass n , soil water w , and surface water h . The model is written as

$$\begin{aligned} \partial_t n &= - \underbrace{\mu n}_{\text{mort.}} + \underbrace{\frac{w}{w+1} n}_{\text{growth}} + \underbrace{\nabla^2 n}_{\text{dispersal}}, \\ \partial_t w &= \alpha \underbrace{\frac{n+f}{n+1} h}_{\text{infil.}} - \underbrace{\nu w}_{\text{evap.}} - \gamma \underbrace{\frac{w}{w+1} n}_{\text{transp.}} + \underbrace{D_w \nabla^2 w}_{\text{diffusion}}, \\ \partial_t h &= \underbrace{p}_{\text{precip.}} - \alpha \underbrace{\frac{n+f}{n+1} h}_{\text{infil.}} + \underbrace{D_h \nabla^2 h}_{\text{diffusion}}, \end{aligned} \quad (1)$$

using the non-dimensional form given by Zelnik *et al.* [11].

In this model, precipitation is a constant input to the surface water field. Surface water infiltrates and becomes soil water. The infiltration rate (i.e. the conversion rate of surface water to soil water) increases in the presence of biomass to model the increased permeability of the soil due to plant roots. Water leaves the soil via evaporation, and is also transpired by plants. The growth rate of biomass is directly proportional to the transpiration rate, and increases with the availability of soil water. Together, these terms make a positive feedback between infiltration and biomass growth: biomass growth increases with soil water, soil water increases with infiltration, and the infiltration rate increases with biomass.

¹Klausmeier [21] uses the mortality rate $M_{tree} = 0.18 \text{ year}^{-1}$ for shrublands and $M_{grass} = 1.8 \text{ year}^{-1}$ for grasslands.

This model includes surface and soil water diffusion terms. Plant dispersal, which encompasses seed dispersal and clonal growth, is also modelled using a diffusion term. The diffusion terms are in two spatial dimensions (2D), i.e. $\nabla^2 = \partial^2/\partial x^2 + \partial^2/\partial y^2$. Surface water diffusion is assumed to occur more rapidly than soil water diffusion, so $D_h > D_w$. Among three-field PDE vegetation models, soil water diffusion and plant dispersal have been modelled as occurring on either similar [14] or different [22] length and time scales, so $D_w \geq 1$. An advection term present in the original form of R02 is neglected here, because the focus of our investigation is on flat-terrain patterns. The dynamics of water on a slope modelled via advection breaks the symmetry that causes 2D patterns such as gaps or spots at pattern onset.

In general, the form of the growth term varies between models [21, 22], and it determines the number of uniform steady state solutions that occur for a given system. For R02, the rate of biomass growth depends linearly on the amount of biomass. The growth rate is also a saturating function of soil water, so that it is linear in the amount of soil water for small values of this variable, and constant for large values. This growth rate permits two steady state solutions, which satisfy the equations

$$\begin{aligned} 0 &= \left(-\mu + \frac{w^*}{w^* + 1}\right) n^*, \\ 0 &= \alpha \frac{n^* + f}{n^* + 1} h^* - \nu w^* - \gamma \frac{w^*}{w^* + 1} n^*, \\ 0 &= p - \alpha \frac{n^* + f}{n^* + 1} h^*. \end{aligned}$$

One solution, $(n^*, w^*, h^*) = (0, p/\nu, p/f\alpha)$, represents a zero-biomass desert state. The other, for which $n^* > 0$ when $p > \mu\nu/1 - \mu \equiv p_0$, represents a vegetated state with nonzero biomass. A diagram of these states as a function of the precipitation parameter is shown in Figure 2. The desert state is stable to spatially uniform perturbations at low values of precipitation ($0 \leq p < p_0$), while the vegetated state is stable to such perturbations at higher values of precipitation ($p > p_0$). These steady states exchange stability in a transcritical bifurcation at $p = p_0$. For a range of precipitation values, indicated by the interval $p \in [p_l, p_u]$, the vegetated state is unstable to spatially periodic perturbations at a range of wavelengths. Pattern-forming instabilities occur at p_l and p_u via the Turing mechanism [18], and we refer to these points as the lower and upper Turing points respectively. These instabilities result in the formation of spatial patterns, which are eventually stabilised by nonlinearities in the system.

As models of dryland vegetation-water interactions, R02 and related models are conceptual in the sense that they are derived using simple mathematical assumptions for the forms of rate and transport terms. For a given parameter set, R02 can be used to generate a corresponding state of the vegetation. The predictions of the model are

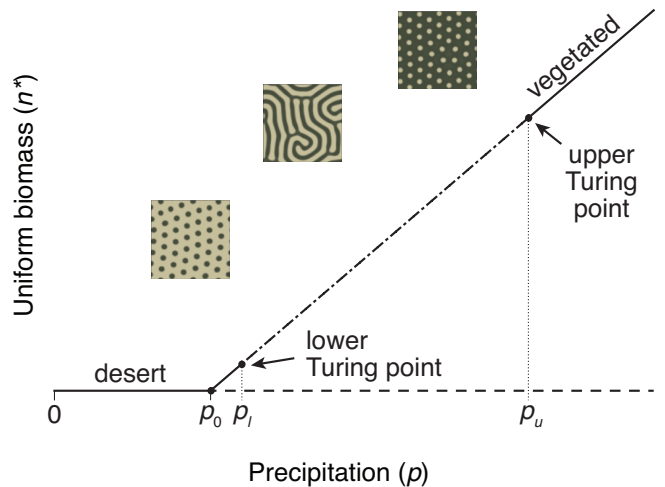


Figure 2: Schematic diagram depicting the uniform steady state solutions of (1), with insets showing examples of patterned states. The uniform desert state is stable on the interval $p \in [0, p_0]$. The desert state exchanges stability with the uniform vegetated state at $p = p_0$, so that the vegetated state is stable to spatially uniform perturbations for $p > p_0$. The vegetated state is unstable to spatially periodic perturbations at a range of wavelengths on the interval $p \in [p_l, p_u]$. We refer to the endpoints p_l and p_u as the lower and upper Turing points, respectively. Examples of patterned states occurring at different values of p are shown using the parameter set given by Zelnik *et al.* [11], which is listed in Table 2. Darker shading denotes higher levels of vegetation biomass.

not considered robust in regimes where the results of calculations are sensitive to a modest variation in the model parameters or in the exact form of the feedbacks used to model interactions. We explore R02 across a range of parameter values to assess the robustness of model behaviours to parameters.

We consider variations of the infiltration rate parameters, f and α . As biomass increases, the infiltration rate approaches α . For low values of biomass, infiltration occurs at the lower rate αf , with $0 < f < 1$. The parameter f controls the strength of the infiltration feedback, where $f = 0$ corresponds to maximal feedback and $f = 1$ corresponds to no feedback. Some soil types have high infiltration rates and are unaffected by the presence of vegetation, while others have low infiltration rates that are more readily influenced. Because of this, it is appropriate to consider a wide range of f and α values in a parameter exploration of R02. We also consider variations of the surface water diffusion rate, D_h . Turing instabilities in R02 occur when plant dispersal and surface water diffusion occur on different scales. The ratio between surface diffusion and plant dispersal rates, D_h , is central to pattern formation, and thus it is varied over a wide range in the investigations in this paper.

2.2 Analysis of patterns and transitions

Pattern formation in R02 (1) and related PDE models is a nonlinear phenomenon and can be studied analytically via bifurcation theory only in certain limits [23, 24]. One such limit occurs in the vicinity of a Turing point [18, 24]. At a Turing point, a uniform steady state has a zero linear growth rate (is neutrally stable) for spatially periodic Fourier mode perturbations of a particular wavelength. We refer to this wavelength as the critical wavelength λ_c , which corresponds to a critical wavenumber $q_c = 2\pi/\lambda_c$. The uniform vegetated state of the R02 model is unstable to Fourier mode perturbations over an interval delimited by two points, which we refer to as the lower and upper Turing points, p_l and p_u respectively. In this investigation, we analyse patterned states via bifurcation theory near these two points by considering only Fourier modes of the solution on a 2D hexagonal lattice [23, 24]. The lattice is constructed so that Fourier modes associated with the critical wavelength grow in a neighbourhood of the Turing point, while all others are linearly damped [25]. A system of six ordinary differential equations (ODEs) for the Fourier mode amplitudes and their complex conjugates can be written to describe the local pattern-forming dynamics of these critical modes. We study the steady states of these ODEs to gain insight into a system's pattern-forming behaviour near the Turing points.

The critical Fourier modes on a hexagonal lattice take the form

$$F_c(\mathbf{x}, t) = z_1(t)e^{i\mathbf{q}_1 \cdot \mathbf{x}} + z_2(t)e^{i\mathbf{q}_2 \cdot \mathbf{x}} + z_3(t)e^{i\mathbf{q}_3 \cdot \mathbf{x}} + c.c.$$

where z_1, z_2 , and z_3 are time-dependent complex amplitudes and *c.c.* denotes the complex conjugates of these amplitudes. $\mathbf{q}_1, \mathbf{q}_2$, and \mathbf{q}_3 are wave vectors such that

$$\mathbf{q}_1 = q_c(1, 0), \quad \mathbf{q}_2 = q_c(-1/2, \sqrt{3}/2), \quad \mathbf{q}_3 = -(\mathbf{q}_1 + \mathbf{q}_2),$$

where q_c is the critical wavenumber. By assuming that pattern dynamics near a Turing point are well-approximated by the modes $F_c(\mathbf{x}, t)$ as a small perturbation to the local uniform steady state, truncated equations for the amplitude dynamics are found to be [23, 26]

$$\begin{aligned} \dot{z}_1 &= \mu z_1 + a\bar{z}_2\bar{z}_3 - (b|z_1|^2 + c(|z_2|^2 + |z_3|^2)) z_1, \\ \dot{z}_2 &= \mu z_2 + a\bar{z}_1\bar{z}_3 - (b|z_2|^2 + c(|z_1|^2 + |z_3|^2)) z_2, \\ \dot{z}_3 &= \mu z_3 + a\bar{z}_1\bar{z}_2 - (b|z_3|^2 + c(|z_1|^2 + |z_2|^2)) z_3. \end{aligned} \quad (2)$$

These equations are considered to be valid in a regime of weak nonlinearity near the Turing point. In this regime, the amplitudes are small so that all three terms contribute to dynamics on the same order. The linear coefficient μ is equivalent to the growth rate of the critical modes obtained by linearising the original system, so that it is small near the Turing point and exactly zero at that point. The quadratic coefficient a must be also small for any steady state solutions to (2) to be stable [26]. The cubic

Table 1: Equations for steady state solutions to (2), and distinct eigenvalues for these solutions. $\mathbf{z} = (z_1, z_2, z_3)$, and $x_s, x_h \in \mathbb{R}^+$.

Solution	Distinct eigenvalues
Gaps (H^-) $\mathbf{z} = -(x_h, x_h, x_h)$ $0 = \mu - ax_h - (b + 2c)x_h^2$	$3ax_h, 0,$ $-ax_h - 2(b + 2c)x_h^2,$ $2ax_h + 2(c - b)x_h^2$
Stripes (S) $\mathbf{z} = (x_s, 0, 0)$ $0 = \mu - bx_s^2$	$-2bx_s^2, 0,$ $-(c - b)x_s^2 + ax_s,$ $-(c - b)x_s^2 - ax_s$
Spots (H^+) $\mathbf{z} = (x_h, x_h, x_h)$ $0 = \mu + ax_h - (b + 2c)x_h^2$	$-3ax_h, 0,$ $ax_h - 2(b + 2c)x_h^2,$ $-2ax_h + 2(c - b)x_h^2$

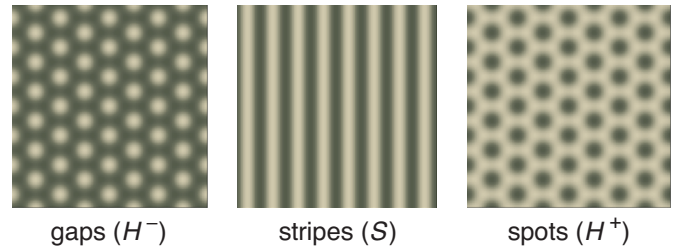


Figure 3: Examples of hexagon (H^- and H^+) and stripe (S) patterns on a 2D hexagonal lattice. We idealise gaps as H^- patterns, labyrinths as S , and spots as H^+ .

coefficients b and c are saturating terms, and also affect the stability of steady state solutions of (2).

Hexagon and stripes steady state solutions of (2) are summarised in Table 1. Hexagon steady states correspond to equal, real-valued amplitudes, with gaps being negative and spots positive. Stripes correspond to the case of only one nonzero amplitude. The stability of these small-amplitude solutions is dictated by the eigenvalues listed in Table 1. Of primary importance to this study is the result that $a < 0$ is a necessary condition for the stability of gaps, and $a > 0$ for spots. The quantities b , $c - b$ and $b + 2c$ are also related to stability and we refer to these in later interpretation of results.

Gap, labyrinth, and spot patterned states have previously been observed in R02 [14]. Examples of these states are shown in Figure 2. We idealise these states as hexagon and stripe steady states on the hexagonal lattice as in [5, 15] (Figure 3). In general, the lower and upper Turing points occur sufficiently far from one another that it is not possible to study transitions between these states via local bifurcation theory in scenarios of changing precipitation. However, Gowda *et al.* [5] consider the special limit in which two Turing points occur near to one another (near to a degenerate Turing point), resulting in pattern transitions that can be analysed via bifurcation theory. In a generic analysis, they find that an analog of the standard “gaps \rightarrow labyrinth \rightarrow spots” sequence is

Table 2: Parameters given by Zelnik *et al.* [11] for the R02 model (1), and parameters varied in this study.

Parameter	Interpretation	Value in [11]	Variation studied
μ	mortality rate	0.5	—
α	infiltration rate	0.4	$10^{-1} - 10^3$
f	infiltration feedback strength	0.2	0.1 - 0.9
ν	evaporation rate	0.4	—
γ	transpiration rate	0.1	—
D_w	ratio of soil water diffusion rate to biomass diffusion rate	1	—
D_h	ratio of surface water diffusion rate to biomass diffusion rate	10^3	$10^{0.5} - 10^4$

one of many possible sequences that can occur as precipitation decreases. They also find that the value of the quadratic a coefficient at the lower and upper Turing acts as a proxy for the apparent pattern sequence. Given conditions on the cubic coefficients that allow the stability of hexagons and stripes solutions to (2), they find that gaps appear at the start of the sequence if $a < 0$ at the upper Turing point. If $a > 0$ at the lower Turing point, then spots appear at the end of the sequence. If these two conditions occur together, then some analog of the standard sequence can occur.

Gowda *et al.* [5] speculated that the quadratic coefficient a provides information about pattern sequences outside the limited setting of a degenerate bifurcation problem. They conducted a bifurcation analysis and small set of numerical simulations on the model by von Hardenberg *et al.* [1] (VH01). VH01 is a two-field PDE vegetation model with cross-diffusion which features two Turing bifurcations on a uniform vegetated steady state (similar to R02). Varying a diffusion coefficient and leaving all other parameters of VH01 fixed, Gowda *et al.* [5] found that $a < 0$ at the upper Turing point and $a > 0$ at the lower Turing point when the diffusion coefficient is sufficiently large. Within this regime, where stable solutions to the amplitude equations exist, the signs of the a coefficient at the Turing points allow pattern sequences to begin with gaps and to end with spots as precipitation decreases. In between these patterns, small-amplitude stripe patterns appear in both analysis and numerical simulations. Where the cubic coefficients b and c prevent the stability of small-amplitude patterns, disordered gaps, labyrinths and spots states were again observed with decreasing precipitation in a numerical simulation. This observation led Gowda *et al.* [5] to speculate that regimes of the model parameter space where the standard sequence occurs are indicated by the a coefficient simply taking a negative sign at the upper Turing point and a positive sign at the lower Turing point, regardless of whether the amplitude equations predict stable patterned states in their small-amplitude regime of validity. Here, we address this question systematically in the R02 model.

3 Methods

We asked whether the quadratic coefficient a of the amplitude equations (2) evaluated at the lower and upper Turing points signals the appearance of the standard sequence in R02 (1). To answer this, we conducted bifurcation analyses and numerical simulations across two relevant parameter spaces of the model.

3.1 Model parameters

We studied variations of the non-dimensional parameter set given by Zelnik *et al.* [11]. These parameter values are summarised in Table 2. The f parameter in R02 controls the strength of the infiltration feedback, and is bounded between 0 and 1. The default value given in [11] is $f = 0.2$. We used $f \in [0.1, 0.9]$ in numerical simulations. The α parameter controls the rate of infiltration, and can take on a range of plausible values depending on the soil type that is modelled. The default value given in [11] is $\alpha = 0.4$, and we considered $\alpha \in [10^{-1}, 10^3]$. The D_h parameter is the ratio of the surface water diffusion rate and the biomass diffusion rate, and can take on a large range of values depending on how surface water transport is interpreted. Rietkerk *et al.* [14] use $D_h = 10^3$ for R02 and Zelnik *et al.* [11] use $D_h = 10^4$ for the corresponding parameter value in a simplified version of the model by Gilad *et al.* [22]. We varied $D_h \in [10^{0.5}, 10^4]$. To consider the dependence of results on co-variation of parameters, we studied the f - α and f - D_h parameter spaces.

3.2 Amplitude equation calculations

We computed coefficients of the amplitude equations (2) for R02 (1) using the procedure outlined in Judd *et al.* [25], which takes a perturbative approach to obtaining these coefficients for a two-field reaction diffusion system. These coefficients are written as expressions of the reaction functions and diffusion parameters. We adapted the Judd *et al.* [25] procedure for a three-field reaction-diffusion system to obtain expressions for the amplitude equation coefficients. The values of the amplitude equation coefficients a , b , and c were computed at the lower and upper Turing points via *Mathematica*. These calculations were performed on a grid of points in the f - α and f - D_h parameter spaces. The results of these calculations

were verified at a few non-degenerate points using a centre manifold reduction approach (the general approach is described in [27]). A Nedler-Mead minimisation library in *Mathematica* was used to find roots of the quantities a , b , $c - b$, and $b + 2c$, which are relevant to assessing the stability of solutions to (2).

3.3 Numerical simulations

We conducted numerical simulations to identify pattern sequences that occur as precipitation decreases in the R02 model (1). We employed a numerical procedure which simulates an ecosystem undergoing a slow monotonic change in precipitation over time. These simulations were run using a grid of parameter values covering a region of the f - α and f - D_h parameter spaces. The procedure is outlined schematically in Figure 4, and is described in depth in the appendix. For each set of parameter values, precipitation is incremented in small discrete steps, and the solution is allowed to reach a steady state between steps. The final state at the previous precipitation value is used as the initial condition for the new precipitation value. The precipitation increment step size was chosen based on the distance between the upper and lower Turing points, $p_u - p_l$, so that approximately 30-100 end states were saved per simulation. Discrete steps were chosen instead of continuously varying precipitation to avoid transient effects, i.e. simulation results that are sensitive to the rate at which precipitation changes.

The procedure is constructed to simulate over the interval of p where patterns are stable and to identify any possible history-dependence (hysteresis) in the pattern sequences. This is accomplished by first incrementing p upward until patterns die out to yield a uniform state. We denote this point of pattern die-off as $p = p_{u+}$. Precipitation is then decremented, simulating a scenario in which an ecosystem slowly becomes more arid. This continues until patterns die out again, which yields another uniform state, which we denote $p = p_{l-}$. Precipitation is incremented upward a final time to assess hysteresis in the pattern sequence (i.e. whether the sequence occurs differently when p is slowly increasing). The procedure terminates when patterns die out once more. An approximate interval for the stability of patterns is given by $p \in (p_{l-}, p_{u+})$. This interval contains the Turing instability interval $p \in [p_l, p_u]$. The Turing instability interval is determined via a linear stability calculation and does not capture the nonlinear stabilisation of patterns. In cases where the amplitude equations (2) predict stable hexagons solutions near a Turing point, these solutions are stable outside the Turing interval. When amplitude equation solutions branch away from the Turing interval (e.g. when stripes bifurcate subcritically), these solutions may also stabilise at large-amplitude outside the Turing interval.

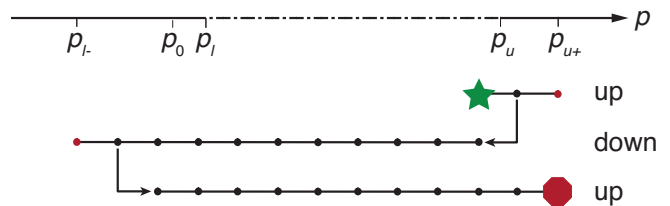


Figure 4: Diagram of numerical simulation procedure. The lower and upper Turing points are marked by p_l and p_u respectively, and p_0 marks the point where the uniform steady states of (1) exchange stability. The dashed line denotes the Turing instability interval $p \in [p_l, p_u]$. Numerical simulations are run at discrete values of p marked by dots. The procedure is initialised at p just below the upper Turing point (star) and run until a steady state is reached. p is then stepped upward by a small increment and once again allowed to reach steady state. This is repeated until patterns lose stability to a uniform vegetated state at $p = p_{u+}$ (red point, right). Using the previous patterned steady state as an initial condition, p is then stepped downward in the same way until patterns lose stability to a uniform state at $p = p_{l-}$ (red point, left). p is incremented upward a final time, and the procedure terminates when patterns once again lose stability (octagon).

4 Results

4.1 Amplitude equation calculations

We find that the f - D_h and f - α parameter spaces of R02 (1) can be divided into regions where the amplitude equations (2) give different qualitative predictions. The results of the calculations at the upper Turing point are summarised in Figure 5, and the lower Turing point calculations are summarised in Figure 6. In the unlabelled white regions, no Turing points occur on the uniform vegetated steady state and no calculations are performed. The black curves separating the white and shaded regions denote a degeneracy of the Turing points, where only one Turing point occurs on the vegetated steady state. In the shaded regions beyond this curve, two Turing points occur on the vegetated state, and analysis is performed at both points.

Each shaded region in Figures 5 and 6 is associated with a qualitatively distinct bifurcation diagram applicable to a neighbourhood of the Turing point. The qualitative aspects (e.g. stability, branching direction) of the bifurcation diagrams are determined by the signs of the quantities a , b , $c - b$, and $b + 2c$. These quantities arise from the amplitude equation steady state eigenvalues and branching equations listed in Table 1. Notably, the sign of the a coefficient serves as a necessary condition for the stability of either small-amplitude gaps or spots solutions. $a < 0$ is a necessary condition for the stability of gaps, and $a > 0$ is a necessary condition for the stability of spots. For the analyses summarised in Figures 5 and 6, the regions are arrayed similarly in both f - D_h and f - α parameter spaces. For example, regions A-E in Figure 5

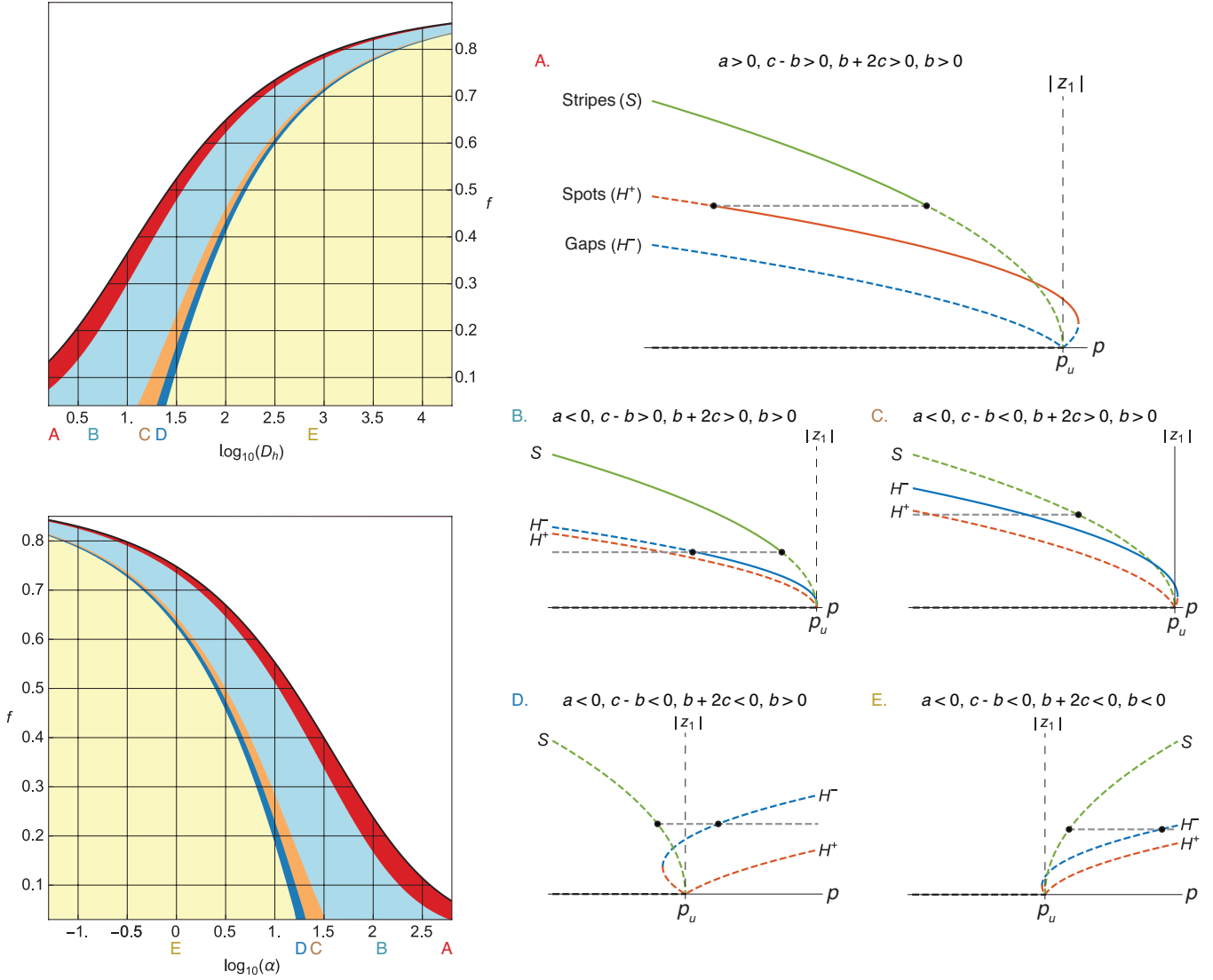


Figure 5: Summary of upper Turing point amplitude equation calculations over f - D_h and f - α parameter spaces, along with schematic bifurcation diagrams. The coefficients of the amplitude equations (2) are computed, and the curves $a = 0$, $b - c = 0$, $c + 2b = 0$, and $b = 0$ separate the parameter spaces into regions labelled A-E. Qualitatively similar bifurcation structures occur within each region. In region A, the conditions a , $c - b$, $b + 2c$, $b > 0$ hold, so the spots (H^+) solution to the amplitude equations is stable in a neighbourhood of the upper Turing point. The stripes solution (S) also stabilises away from the Turing point. These solutions are depicted in bifurcation diagram A. In region B, both gaps (H^-) and stripes solutions can be stable, whereas in region C, the small-amplitude stripes solution cannot be stable. In regions D-E, no solutions to the amplitude equations can be stable. These two regions differ only in the branching direction of the stripes solution branch, which switches when b changes sign. In the white region, no Turing points occur on the uniform vegetated steady state of R02 (1) and no calculations are performed.

occur in the same order when varying parameters away from the Turing degeneracy curve (e.g. when increasing D_h with f fixed compared to decreasing α with f fixed).

We first interpret the results of bifurcation analysis at the upper Turing point, which are summarised in Figure 5. We consider a scenario in which precipitation decreases slowly over time, so that the upper Turing point threshold is crossed from above. The sequence of pattern morphologies observed in such a scenario begin with patterns born near the upper Turing point. The regions in Figure 5 specify whether the amplitude equations predict a stable patterned state near the upper Turing point, and also the morphology of that state. A gap (H^-) patterned state stable near the upper Turing point accords with the standard “gaps \rightarrow labyrinth \rightarrow spots” sequence prediction.

In region A of Figure 5, the quantities a , $c - b$, $b + 2c$, and b are all positive, which allows a stable spot solution (H^+) to the amplitude equations near the upper Turing point. This analysis predicts that pattern sequences begin with spot patterns in region A of the parameter space. Such sequences are inconsistent with the standard sequence prediction. The stripes solution (S) can also be stable in region A. These solutions stabilise away from the Turing point, so that spots may transition to stripes as precipitation decreases. However, since the predictions of the amplitude equations break down outside a small neighbourhood of the Turing point, it is uncertain whether this stable stripes solution manifests in the full system as a successor to spot patterns as precipitation decreases.

In regions B and C of Figure 5, a is negative and $b + 2c$ and b are positive, which allows a stable gaps solution to the amplitude equations near the upper Turing point. This predicts pattern sequences that begin with gap patterns. Such sequences are consistent with the standard sequence. The stripes solution to the amplitude equations can also be stable in region B, as in region A, since $c - b > 0$. Here, gap patterns may transition to stripes as precipitation decreases. In region C, $c - b < 0$ prevents the stability of stripe steady states. The analysis therefore provides no information in this region about the patterns that follow gaps as precipitation decreases.

In regions D and E of Figure 5, a , $c - b$, and $b + 2c$ are negative, which means steady state solutions to the amplitude equations are never stable near the upper Turing point. Regions D and E differ only by the branching direction of the always-unstable stripes solution. The stripes solution branches towards the Turing instability interval (i.e. stripes bifurcate supercritically) for region D, since $b > 0$. The stripes solution branches away from the Turing instability interval (i.e. stripes bifurcate subcritically) for region E, since $b < 0$. In both D and E, the hexagon solutions branch away from the Turing instability region. Since there are no stable steady states of the amplitude equations in regions D and E, we cannot directly infer from this analysis what patterned states occur near the

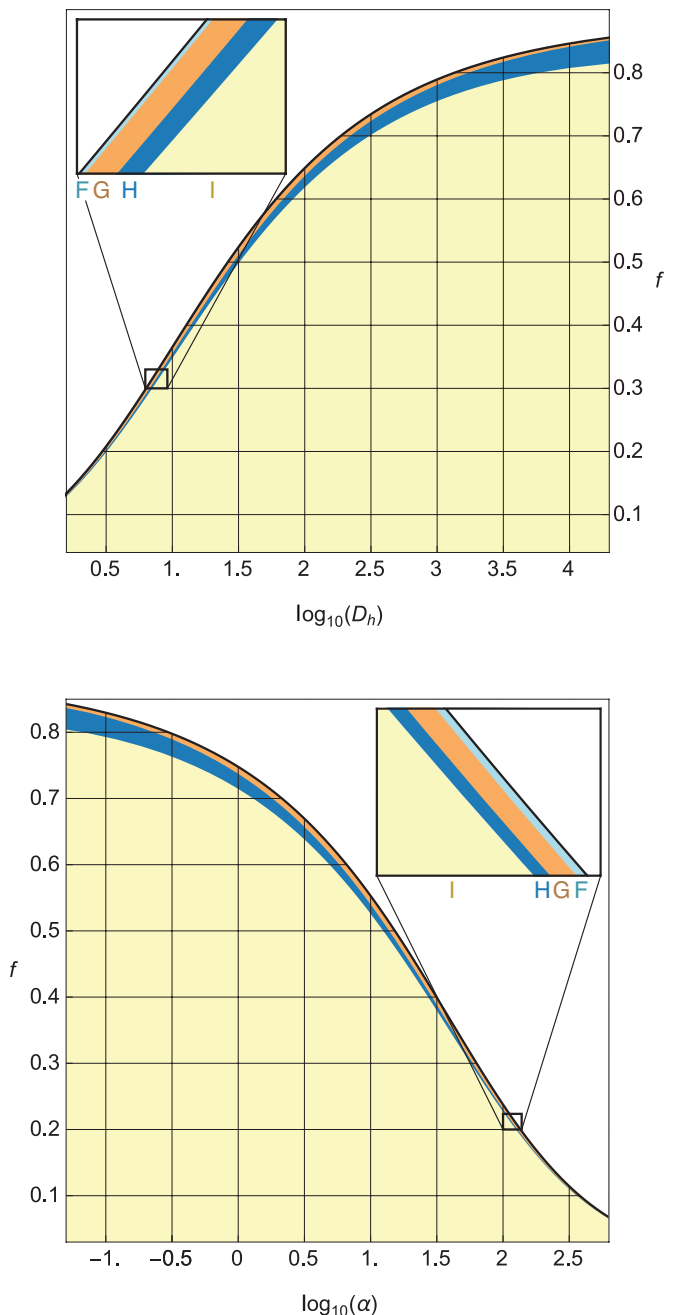


Figure 6: Summary of lower Turing point amplitude equation calculations over f - D_h and f - α parameter spaces. The coefficients of the amplitude equations (2) are computed, and the curves $c - b = 0$, $b + 2c = 0$, and $b = 0$ separate the parameter space into regions labelled F-I, each of which exhibits a qualitatively distinct bifurcation structure. Regions F-H are tightly clustered near the Turing degeneracy curve (black line). In region F, the spots solution to the amplitude equations is stable in a neighbourhood of the lower Turing point. The stripes solution also stabilises away from the Turing point in this region. In region G, only the spots solution can be stable. In regions H and I, no solutions to the amplitude equations can be stable. These two regions differ only in the branching direction of the stripes solution, which switches when b changes sign. Bifurcation diagrams applicable to regions F-I resemble diagrams B-E in Figure 5, with the roles of gaps and spots exchanged and the solutions reflected across the $|z_1|$ axis.

Turing point. Here, patterned states of the full system likely arise from more strongly nonlinear behaviour than the states in regions A-C.

Figure 6 summarises the results of bifurcation analysis at the lower Turing point. Over the entire f - D_h and f - α parameter spaces, a is positive, which is a necessary condition for the stability of spot solutions to the amplitude equations. Regions F-H all occur in close proximity to the degenerate Turing point curve, while region I fills the majority of the space. Stable solutions to the amplitude equations occur only in regions F and G. In region F, the spots solution to the amplitude equations is stable near the lower Turing point. The stripes solution is also stable away from the Turing point in this region, so that spots may transition to stripes as precipitation increases. In region G, the spots solution is stable near the lower Turing point, but the stripes solution can never be stable. In regions H and I, solutions to the amplitude equations are never stable near the lower Turing point, and differ only in the branching direction of the stripes solution. The stripes solution branches towards the Turing instability region for region H, and away for region I.

At both the upper and lower Turing points, our bifurcation analysis cannot provide direct information about stable patterned states for a large region of the parameter space, where small-amplitude solutions are unstable. The central investigation of this paper is whether the a coefficient, obtained via local analysis, contains information about patterned states near the Turing points in these other regions. In regions B and C of Figure 5, it is expected from the analysis that gap patterns are stable near the upper Turing point. We posit that the same is true in regions D and E, where no solutions to the amplitude equations are stable, but $a < 0$. Similarly, our analysis only shows that spot patterns are stable near the lower Turing point in regions F and G of Figure 6. We posit that spots patterns will be stable near the lower Turing point in regions H and I as well, since $a > 0$ there. In a scenario of decreasing precipitation over time, we expect to see pattern sequences that begin with gaps and end with spots (i.e. analogs of the standard sequence) in the region of parameter space where $a < 0$ at the upper Turing point and $a > 0$ at the lower Turing point. We find that these conditions are satisfied over nearly all of the studied f - α and f - D_h parameter spaces, excluding only region A of Figure 5. In region A, $a > 0$ at the upper Turing point and we expect pattern sequences that begin and end with spots.

4.2 Numerical simulations

We find that the a coefficient of the amplitude equations (2) signals where the standard sequence occurs in the studied parameter spaces of R02 (1). A summary of pattern sequences observed in numerical simulations is shown in Figure 7. Numerical simulations were conducted as described in Section 3.3 and the appendix at

sets of parameter values marked by letters, and pattern sequences were identified by visual inspection. The region of the parameter space where $a > 0$ at both the upper and lower Turing points (i.e. region A of Figure 5) is shaded. Elsewhere, $a < 0$ at the upper Turing point and $a > 0$ at the lower Turing point. In the analysis described in Section 4.1, we determine that pattern sequences beginning with spots (in a scenario of decreasing precipitation) should appear in the shaded region. Outside the thin shaded region, we expect to see analogues of the standard sequence. We find that both of these expectations generally hold in numerical simulations. Only spot patterned states are observed in the shaded region, while analogues of the standard sequence are primarily observed elsewhere. Figure 7 also shows examples of the numerical patterned states using $f = 0.2$ and different values of $\log_{10}(D_h)$. The simulation output is accompanied by number lines which plot the locations of the upper and lower Turing points (p_u and p_l respectively), the transcritical point (p_0), and upper and lower pattern stability boundaries (p_{u+} and p_{l-} , described in Section 3.3).

We observed only spot patterned states in the thin shaded region of Figure 7. Example simulation output from $f = 0.2$ and $\log_{10}(D_h) = 0.6$ demonstrating this sequence is shown. This result agrees with our analysis at the upper Turing point and our expectation for behaviour near the lower Turing point. Near the upper Turing point, solutions approximately resemble the spots (H^+) solution to the amplitude equations (2) shown in Figure 3. The profiles of these spot patterns are roughly sinusoidal about the uniform vegetated steady state. An example sinusoidal profile is shown in Figure 8. At lower values of p , spot patterns remain stable. The spacing between spots increases, and the individual spots of vegetation become more sharply peaked, quickly decaying to zero away from the centre of a spot. An example of a sharply peaked profile is also shown in Figure 8. Patterns other than spots are not observed in simulations conducted in the shaded region. No notable hysteresis in the qualitative appearance of the spot patterns was observed as precipitation increased in discrete steps.

We primarily observed analogues of the standard “gaps \rightarrow labyrinths \rightarrow spots” sequence in the unshaded region of Figure 7, which also agrees with our expectations from analysis. Examples of this sequence in simulation output for $f = 0.2$ and $\log_{10}(D_h)$ ranging from 1.0 – 4.0 are shown in Figure 7. The set of simulations at $\log_{10}(D_h) = 1.0$ uses a parameter set from region B of Figure 5, where gaps solutions to the amplitude equations are expected to be stable near the upper Turing point, and stripes solutions can also stabilise nearby. As precipitation decreases in the simulations, patterns resembling the gaps (H^-) solution to the amplitude equations are first observed near the upper Turing point. Gaps then transition to well-ordered stripe patterns of a relatively small amplitude (≈ 0.35). As precipitation decreases further, stripes become disordered in a zig-zag manner before

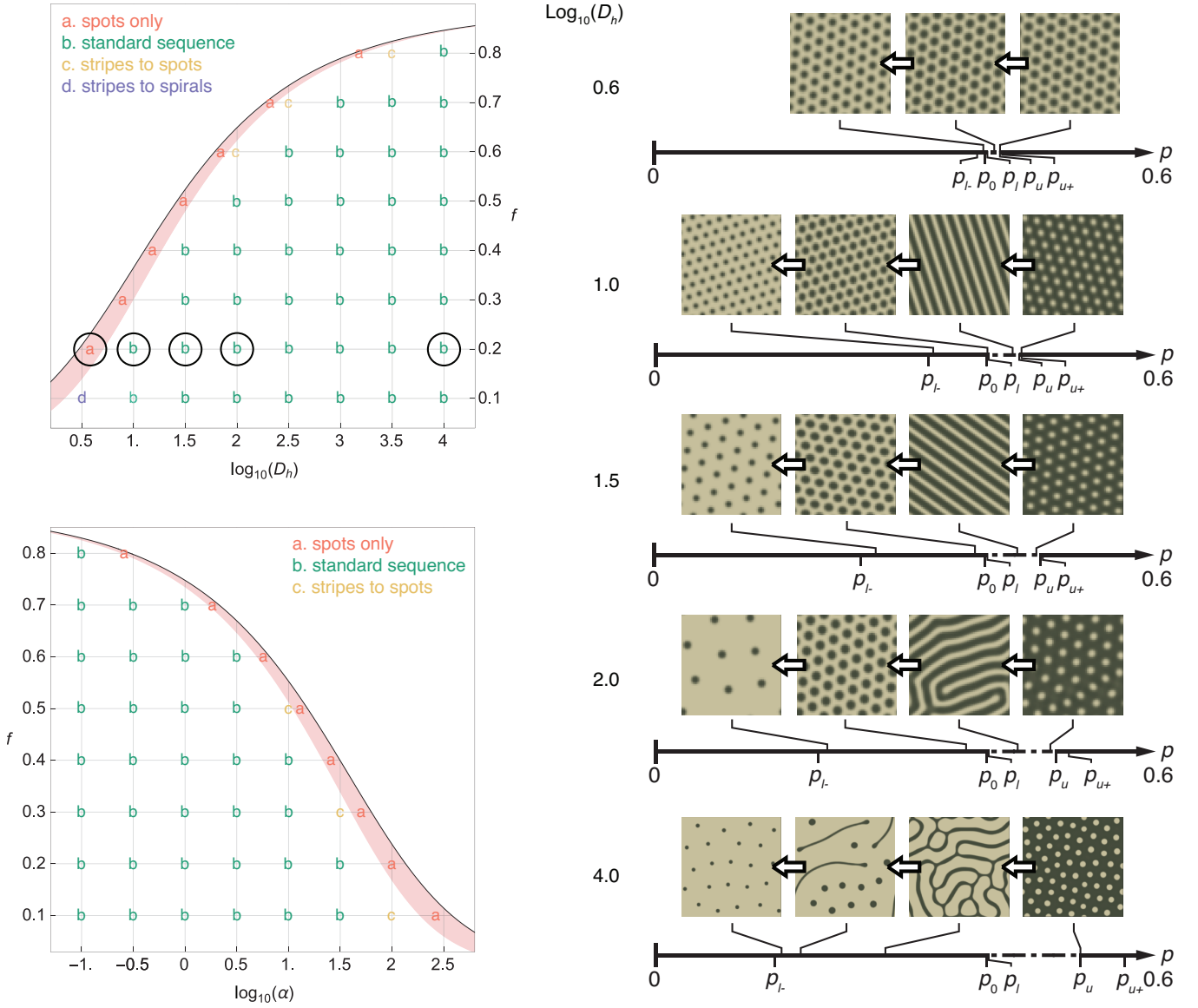


Figure 7: Summary of pattern transitions observed numerical simulations over f - D_h and f - α parameter spaces in R02 (1), along with representative examples of transitions from numerical simulations at $f = 0.2$ and $\log_{10}(D_h) = 0.6 - 4.0$. In the shaded region, $a > 0$ at both the upper and lower Turing points. Only spot patterns are observed in this region. Elsewhere, $a < 0$ at the upper Turing point and $a > 0$ at the lower Turing point. The standard sequence is primarily observed here. Stripes to spots and stripes to spirals sequences are also observed in a few instances (examples of the latter are shown in Figure 9). Number lines plot the relative locations of the upper and lower Turing points (p_u and p_l respectively), the transcritical point (p_0), and upper and lower pattern stability boundaries (p_{u+} and p_{l-}) for the example simulations shown. The parameter values corresponding to the example simulations are circled. Though p_l and p_0 are nearly coincident, the distance between these points is exaggerated to illustrate that $p_l > p_0$.

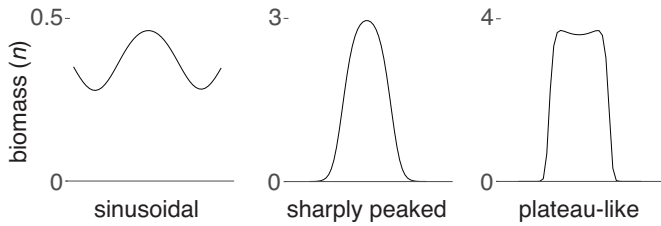


Figure 8: Example profiles of individual spot patterns taken from numerical simulations at $f = 0.2$ and $\log_{10}(D_h) = 0.6$ (sinusoidal), $\log_{10}(D_h) = 2.0$ (sharply peaked), and $\log_{10}(D_h) = 4.0$ (plateau-like). The example sinusoidal profile comes from a spot patterned state near the upper Turing point. The sharply peaked and plateau-like profiles come from spot patterned states well below the lower Turing points in their respective simulations.

transitioning to spot patterns. The vegetation spots decrease in size with decreasing precipitation before finally collapsing to a uniform desert state. As with the spots in the set of simulations at $\log_{10}(D_h) = 0.6$, spots become less sinusoidal in profile and more sharply peaked as precipitation decreases. When increasing precipitation, gap patterns do not reappear after stripes. Spots transition to stripes, which remain stable until $p = p_{u+}$. No notable hysteresis occurs in the points of transition between patterns in this set of simulations.

The simulations at $\log_{10}(D_h) = 1.5$ use a parameter set from region C of Figure 5, where small-amplitude gaps are expected to be stable near the upper Turing point, but small-amplitude stripes solutions cannot be stable. In the simulations, a small-amplitude gaps pattern is indeed observed near the upper Turing point. As precipitation decreases, gap patterns transition to a well-ordered stripe pattern. In contrast to the well-ordered stripes observed at $\log_{10}(D_h) = 1.5$, these stripes have an approximately $\mathcal{O}(1)$ amplitude. Ordered stripes then become disordered in a zig-zag manner before transitioning to spots. The spots decrease in radius with precipitation, and eventually coarsen to yield a pattern with a larger wavelength before collapse to a desert state. A “spots \rightarrow stripes \rightarrow gaps” sequence occurs (i.e. the standard sequence occurs in reverse) when increasing precipitation. Hysteresis occurs in the transition between stripes and spots. This transition occurs at a slightly lower value of p when decreasing precipitation compared to when increasing precipitation.

The simulations at $\log_{10}(D_h) = 2.0$ use a parameter set from region E of Figure 5, where no small-amplitude patterns are expected to be stable near the upper Turing point. Still, gaps are observed in numerical simulations near the upper Turing point. As precipitation decreases, gaps transition directly to disordered labyrinthine stripes. The labyrinth patterns then transition to spots via intermediate states in which spots and stripes appear to coexist. As precipitation decreases further, the radii of vegetation spots shrink and the pattern coarsens be-

fore collapsing. The profiles of gaps, labyrinths and spots in these simulations begin to diverge from the sinusoidal forms observed at smaller values of $\log_{10}(D_h)$ (Figure 8). Gaps appear as sharp punctures to a flat vegetation state and stripes decay rapidly to zero in inter-stripe areas. All spots take on strongly peaked profiles in these simulations. When increasing precipitation, the standard sequence occurs in reverse. The transitions between gaps and labyrinths occur at a lower value of p when decreasing precipitation compared to increasing precipitation. The same applies to the transition between labyrinths and spots.

The simulations at $\log_{10}(D_h) = 4.0$ also use a parameter set from region E of Figure 5. Gaps are observed in numerical simulations near the upper Turing point. The transition from gaps to stripes with decreasing precipitation occurs via an intermediate phase in which gaps and stripes appear to coexist. The stripes state that follows is qualitatively different from the other stripe states shown for lower values of $\log_{10}(D_h)$. The state is distinctly labyrinthine, featuring thin stripes of vegetation surrounded by large bare ground areas. As with $\log_{10}(D_h) = 2.0$, the labyrinth patterns transition to spots via intermediate states in which spots and stripes appear to coexist. Finally, spots shrink and coarsen before collapsing as precipitation decreases further. The profiles of gaps, labyrinth and spot patterns are quite different in this set of simulations than those discussed at lower values of $\log_{10}(D_h)$. Within each patterned state, the transition between vegetation and bare areas occurs sharply. For example, this causes spot patterns to take on a plateau-like profile (Figure 8). When increasing precipitation, the standard sequence occurs in reverse, with apparent coexistence of spots/stripes and gaps/stripes occurring at intermediate points. The transition point between pure spots and spots/stripes coexistence states occurs at a lower value of p when decreasing precipitation compared to increasing precipitation. The same is observed for the transition point between pure gaps and gaps/stripes.

These simulation examples demonstrate a trend of increasingly nonlinear behaviour as D_h increases. This trend is generally representative of what we observe in other simulations when parameters are varied away from the Turing degeneracy curve. One aspect of the increasing nonlinearity can be accounted for via our bifurcation analysis. The regions in Figure 5 order the parameter space by nonlinearity at the upper Turing point. Moving away from the Turing degeneracy curve, the amplitude equations first predict weakly nonlinear patterns in regions A-C, and then imply strongly nonlinear patterns in regions D and E. This manifests in simulations as small-amplitude sinusoidal patterns occurring near the upper Turing point when parameters are near to the Turing degeneracy curve, sharply peaked patterns occurring beyond this, and plateau-like patterns occurring when very far away from the curve. Other aspects of increasing non-

linearity are apparent in certain qualitative behaviours observed in the simulations. Patterned states increase in their disorder and begin to exhibit coexistence as distance from the degeneracy curve increases. The interval of pattern stability, $[p_{l-}, p_{u+}]$, increases in length as well. In particular, p_{l-} decreases to extend the length of the interval $[p_{l-}, p_l]$. As this interval increases with increasing distance from the Turing degeneracy curve, the transition point between stripes and spots states decreases to lower values of precipitation. This causes spot patterns to develop at values of precipitation well below the lower Turing point. This implies the stabilisation of a strongly nonlinear patterned state far from the Turing instability interval.

Aside from the standard sequence, we observed a few instances of “stripes \rightarrow spots” sequences in the unshaded region of Figure 7. We determined that these are actually instances of the standard sequence, where gaps do not appear in simulations. Our bifurcation analysis indicates that gap solutions to the amplitude equations should be stable near the upper Turing point (region B of Figure 5). When a is sufficiently small, as it may be for the “stripes \rightarrow spots” observations, the gaps solution is stable for only a relatively small interval of the precipitation parameter compared to the stripes branch. This is illustrated schematically in bifurcation diagram B in Figure 5. Because our numerical procedure increments precipitation in discrete steps of fixed size, the gaps branch may be bypassed. Also, since gaps are stable only very near to the Turing point for these parameter sets, gaps may only be stable at the critical wavelength and may not appear in a domain of arbitrary size. To test whether gaps can exist stably for parameter sets where “stripes \rightarrow spots” transitions are observed, we seeded numerical simulations at $p = p_u$ with a hexagonal lattice gaps pattern at the critical wavelength. This initial condition was also perturbed by a small amount of spatially random noise. An aspect ratio of $1 : \sqrt{3}$ and a domain size that permits an integer multiple of the critical wavelength were used. In all simulations, gap patterns persisted as steady states through $t = 1 \times 10^6$ and were assessed to be stable in these instances.

We also observed time-varying spiral wave patterns in one instance of the numerical simulations, at $f = 0.1$ and $\log_{10}(D_h) = 0.5$. Example states from this set of simulations are shown in Figure 9. We verified that the observation of spirals is robust to increased spatial and temporal resolution in the numerical scheme. We ran additional simulations at nearby parameter values and found that spirals patterns appear to be confined to small values of f and D_h . Holding $f = 0.1$ fixed, spirals appear in simulations at $\log_{10}(D_h) = 0.6$ but not $\log_{10}(D_h) = 0.7$. Holding $\log_{10}(D_h) = 0.5$ fixed, spirals appear at $f = 0.16$ but not at $f = 0.18$. Spirals are thus observed at values of D_h that are smaller than typically considered reasonable. To our knowledge, there are no previous reports of spiral wave patterns occurring in R02 or any other

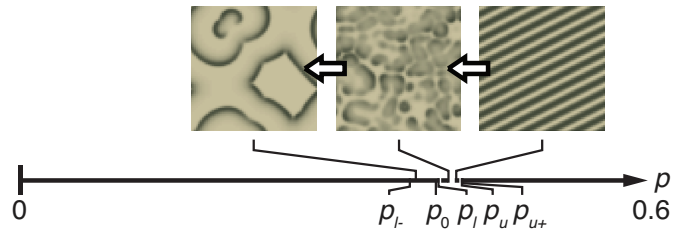


Figure 9: Spiral wave patterns are observed in simulations at $f = 0.1$ and $\log_{10}(D_h) = 0.5$. An ordered stripes state transitions directly to spirals at $p = 0.414$.

vegetation model. However, the waves observed in R02 resemble spiral wave patterns observed in other reaction-diffusion contexts such as chemical reaction systems [28] and models of phytoplankton dynamics [29].

5 Discussion

We find that the quadratic coefficient a from a 2D bifurcation analysis divides the studied parameter spaces into two regions. In a thin region of the parameter space adjacent to the degenerate Turing point curve, a is positive at both Turing points, and we observe only spot patterns in numerical simulations. Elsewhere a takes opposite signs at the two Turing points, and we primarily observe the standard sequence. This strongly suggests that the a coefficient holds predictive value for identifying the standard sequence in the R02 parameter space. Since a is computed analytically, it is possible to trace the influence of model terms and parameter values on the value of the coefficient. This presents not only an approach for comprehensively exploring the full 7-dimensional parameter space of the R02 model, but also an opportunity to understand the role of ecological processes on the highly nonlinear phenomenon of pattern transitions in dryland vegetation models. We find that the standard sequence occurs over the vast majority of the parameter space studied. This points to some underlying model structure, perhaps in the nature of the infiltration feedback or in the form of the transpiration term, that supports the occurrence of the “gaps \rightarrow labyrinths \rightarrow stripes” sequence as precipitation decreases. Dissecting the a coefficient to determine which model terms most significantly influence its value offers a way to understand this structure in R02, and perhaps even in a more general class of PDE vegetation models. This is an ongoing direction of study in our investigation of PDE vegetation models.

Not all PDE vegetation models feature two Turing points on the vegetated steady state. The Klausmeier Gray-Scott model [12, 21] and Simplified Gilad model [4, 11, 22] (in the parameter regime typically studied) have only one Turing point on the vegetated steady state, which corresponds in some sense to the upper Turing point in R02. For a more general class of vegetation models, two Turing points can be expected typically when

the uniform vegetated steady state bifurcates transcritically from the desert state and when this state is stable for low levels of vegetation. This generically occurs when the transcritical bifurcation is supercritical. A description of Turing points in this general class of vegetation models is given by Iams *et al.* [30]. In the analysis of R02 conducted here, the information used to divide the parameter space into regions with different expected transition behaviours was encoded into the upper Turing point. The lower Turing point remained positive throughout the parameter space studied, and spot patterns were always observed in simulations at low levels of precipitation. It therefore may be true that in vegetation models with only one Turing point, the sign of the a coefficient at this point is sufficiently informative to predict where the standard sequence occurs in the parameter space. If so, this would represent another remarkable simplification which permits the analysis of pattern transitions in PDE vegetation models.

Much recent work focuses on the potential for early warning signs in ecological systems in general [16, 31]. We take the perspective that a prediction must be demonstrated robust within a modelling framework to be considered a candidate early warning sign. We have explored one type of robustness—to parameter variation within a model—and suggested an approach for studying robustness to model formulation. Still, there lie other challenges to assessing the viability of early warning signs under model changes which increase realism. Dryland environments are heterogeneous in both space and time [32]. The effect of spatial anisotropy via a slope of constant grade disrupts the formation of gap and spot patterns [33]. It is unknown how further, more disordered anisotropy affects the formation of spatial patterns and the appearance of the standard sequence. It is also unclear what rates of parameter change are relevant and whether the observed pattern morphologies are sensitive to this rate [34]. Despite these challenges, we believe it is useful to begin studying robustness in an idealised setting, and to perturb outward from this setting. Doing so mitigates the substantial complexity of real world ecosystems within a framework where modifications can be articulated and tested.

Acknowledgements

The authors benefitted from useful conversations at the “Spatio-Temporal Dynamics in Ecology” workshop at the Lorentz Centre (Leiden, NL, December 2014). Research was supported in part by the NSF Math and Climate Research Network (DMS-0940262).

Appendix

Details of numerical simulations

We numerically solved the R02 model (1) using the exponential time differencing Runge-Kutta 4 (ETDRK4) scheme [35, 36] modified for 2D systems [37]. ETDRK4 achieves pseudospectral accuracy in space and fourth-order accuracy in time. This scheme alleviates issues of stiffness often associated with reaction-diffusion systems [37], allowing R02 to be simulated efficiently. Simulations were run using a time step near to the scheme’s empirically derived stability limit, since our primary concern is with qualitative aspects of patterned solutions. This scheme was implemented in MATLAB and C.

For each set of parameter values marked by a letter in Figure 7, we simulated R02 over a range of precipitation values using a procedure summarised in Section 3.3 and described in detail here. Simulations are initialised with a spatially random initial condition beginning just below the upper Turing point, at $p = p_l + 0.95(p_u - p_l)$. Then, the following loop is run to identify the upper bound of pattern stability:

1. R02 is solved using ETDRK4 until either a steady state stop condition or a uniformity stop condition is reached. The end state of the simulation is saved.
2. If the steady state stop condition was reached, precipitation is incremented **upward** by a small value Δp . The procedure returns to step 1, using the saved end state as the initial condition for a new simulation. If the spatial uniformity stop condition was reached, the loop ends.

The steady state stop condition occurs when either (a) the root mean square difference between the current biomass state and the state 400 time units earlier drops below 10^{-4} , or (b) $t = 2 \times 10^5$. The uniformity stop condition occurs when the root mean square difference between the current biomass state and the mean value of that state drops below 10^{-4} . We infer the upper bound of pattern stability, p_{u+} , to be the value of precipitation when the uniformity condition is reached.

After the first loop terminates and the first uniformity condition is reached, precipitation is incremented downward by $2\Delta p$. The previous patterned (i.e. non-uniform) end state is used as the initial condition for a new simulation. We run the following loop to identify pattern morphologies that occur as precipitation decreases:

1. R02 is solved using ETDRK4 until a stop condition is reached. The end state of the simulation is saved.
2. If a steady state stop condition is reached, precipitation is incremented **downward** by Δp and the procedure returns to step 1, using the saved end state as the initial condition for a new simulation. If the spatial uniformity stop condition is reached, the loop ends.

When this loop ends, we infer the lower bound of pattern stability, p_{l-} , to be the value of precipitation when the uniformity condition is reached.

We increment precipitation upward in one final loop to identify any potential hysteresis effects. Precipitation is first incremented upward by $2\Delta p$. The previous patterned (non-uniform) end state is used as the initial condition for a new simulation. Then the following loop is run:

1. R02 is solved using ETDRK4 until a stop condition is reached. The end state of the simulation is saved.
2. If a steady state stop condition is reached, precipitation is incremented **upward** by Δp and the procedure returns to step 1, using the saved end state as the initial condition for a new simulation. If the spatial uniformity stop condition is reached, the loop ends.

The end result of this procedure is a series of saved end states at a range of precipitation values over the interval $p \in [p_{l-}, p_{u+}]$.

The precipitation iteration step size Δp was chosen based on the distance between the upper and lower Turing points, $p_u - p_l$, so that 30-100 end states were saved per parameter set. The value of Δp used ranged between 0.01 and 0.0025. For most simulations, a time step size of $\Delta t = 0.4$ was used, which was near the empirical stability limit of the scheme for most parameter sets. On certain parameter sets, values of Δt as small as 0.01 were needed for numerical stability. We tested for time step size errors using a particular parameter set, with $\Delta t = 0.4, 0.2,$ and $0.1,$ and the end states were found to be qualitatively indistinguishable. A preliminary set of simulations was run on all parameter sets to identify a simulation domain size for each that permits at least 7 wavelengths of patterns. Square $L \times L$ domains with $L = 400, 800,$ and 1600 were used. Corresponding $N \times N$ grid sizes were used, with $N = 64, 128,$ and 256 respectively.

References

- [1] Jost von Hardenberg, Ehud Meron, Moshe Shachak, and Yair Zarmi. Diversity of Vegetation Patterns and Desertification. *Physical Review Letters*, 87(19):198101, October 2001.
- [2] Golan Bel, Aric Hagberg, and Ehud Meron. Gradual regime shifts in spatially extended ecosystems. *Theoretical Ecology*, 5(4):591–604, January 2012.
- [3] Vasilis Dakos, Sonia Kéfi, Max Rietkerk, Egbert H van Nes, and Marten Scheffer. Slowing Down in Spatially Patterned Ecosystems at the Brink of Collapse. *The American Naturalist*, 177(6):E153–E166, June 2011.
- [4] Erez Gilad, Jost von Hardenberg, Antonello Provenzale, Moshe Shachak, and Ehud Meron. Ecosystem engineers: from pattern formation to habitat creation. *Physical Review Letters*, 93(9):098105, 2004.
- [5] Karna Gowda, Hermann Riecke, and Mary C Silber. Transitions between patterned states in vegetation models for semiarid ecosystems. *Physical Review E*, 89(2):022701, 2014.
- [6] Vishwesh Guttal and Ciriya Jayaprakash. Self-organization and productivity in semi-arid ecosystems: Implications of seasonality in rainfall. *Journal of Theoretical Biology*, 248(3):490–500, October 2007.
- [7] Sonia Kéfi, Maarten B Eppinga, Peter C de Ruiter, and Max Rietkerk. Bistability and regular spatial patterns in arid ecosystems. *Theoretical Ecology*, 3(4):257–269, January 2010.
- [8] Olivier LeJeune, Mustapha Tlidi, and Pierre Couteron. Localized vegetation patches: A self-organized response to resource scarcity. *Physical Review E*, 66(1):010901, July 2002.
- [9] Ehud Meron, Erez Gilad, Jost von Hardenberg, Moshe Shachak, and Yair Zarmi. Vegetation patterns along a rainfall gradient. *Chaos, Solitons & Fractals*, 19(2):367–376, January 2004.
- [10] Jonathan A Sherratt. Using wavelength and slope to infer the historical origin of semiarid vegetation bands. *Proceedings of the National Academy of Sciences*, page 201420171, March 2015.
- [11] Y R Zelnik, S Kinast, and Hezi Yizhaq. Regime shifts in models of dryland vegetation. *Proceedings of the Royal Society A: Mathematical, Physical and Engineering Science*, 2013.
- [12] Sjors van der Stelt, Arjen Doelman, Geertje Hek, and Jens DM Rademacher. Rise and fall of periodic patterns for a generalized Klausmeier–Gray–Scott model. *Journal of Nonlinear Science*, 23(1):39–95, 2013.
- [13] K Siteur, E Siero, M B Eppinga, and JDM Rademacher. Beyond Turing: The response of patterned ecosystems to environmental change. *Ecological Complexity*, 2014.
- [14] Max Rietkerk, Maarten C Boerlijst, Frank van Langevelde, Reinier HilleRisLambers, Johan van de Koppel, Lalit Kumar, Herbert HT Prins, and André M de Roos. Selforganization of vegetation in arid ecosystems. *The American Naturalist*, 160(4):524–530, 2002.
- [15] Olivier LeJeune, Mustapha Tlidi, and René Lefever. Vegetation spots and stripes: Dissipative structures in arid landscapes. *International Journal of Quantum Chemistry*, 98(2):261–271, 2004.

- [16] Max Rietkerk, Stefan C Dekker, Peter C de Ruiter, and Johan van de Koppel. Self-organized patchiness and catastrophic shifts in ecosystems. *Science*, 305(5692):1926–1929, 2004.
- [17] Marten Scheffer, Jordi Bascompte, William A Brock, Victor Brovkin, Stephen R Carpenter, Vasilis Dakos, Hermann Held, Egbert H van Nes, Max Rietkerk, and George Sugihara. Early-warning signals for critical transitions. *Nature*, 461(7260):53–59, 2009.
- [18] A M Turing. The Chemical Basis of Morphogenesis. *Philosophical Transactions of the Royal Society of London. Series B, Biological Sciences*, 237(641):37–72, August 1952.
- [19] Nicolas Barbier, Pierre Couteron, Jean LeJoly, Vincent Deblauwe, and Olivier LeJeune. Selforganized vegetation patterning as a fingerprint of climate and human impact on semiarid ecosystems. *Journal of Ecology*, 94(3):537–547, 2006.
- [20] Vincent Deblauwe, Pierre Couteron, Olivier LeJeune, Jan Bogaert, and Nicolas Barbier. Environmental modulation of self-organized periodic vegetation patterns in Sudan. *Ecography*, 34(6):990–1001, July 2011.
- [21] Christopher A Klausmeier. Regular and irregular patterns in semiarid vegetation. *Science*, 284(5421):1826–1828, 1999.
- [22] Erez Gilad, Jost von Hardenberg, Antonello Provenzale, Moshe Shachak, and Ehud Meron. A mathematical model of plants as ecosystem engineers. *Journal of Theoretical Biology*, 244(4):680–691, February 2007.
- [23] Rebecca Hoyle. *Pattern Formation: An Introduction to Methods (Cambridge Texts in Applied Mathematics)*. Cambridge University Press, first edition, April 2006.
- [24] Michael Cross and Henry Greenside. *Pattern Formation and Dynamics in Nonequilibrium Systems*. Cambridge University Press, 1 edition, August 2009.
- [25] Stephen L Judd and Mary C Silber. Simple and superlattice Turing patterns in reaction–diffusion systems: bifurcation, bistability, and parameter collapse. *Physica D: Nonlinear Phenomena*, 136(1):45–65, 2000.
- [26] Martin Golubitsky, Ian Stewart, and David G Schaeffer. *Singularities and Groups in Bifurcation Theory*. Springer Verlag, July 2012.
- [27] Stephen Wiggins. *Introduction to Applied Nonlinear Dynamical Systems and Chaos*. Springer, October 2003.
- [28] Vladimir K Vanag. Waves and patterns in reaction–diffusion systems. Belousov–Zhabotinsky reaction in water-in-oil microemulsions. *Physics-Uspekhi*, 47(9):923–941, October 2007.
- [29] Horst Malchow, Frank M Hilker, Sergei V Petrovskii, and Klaus Brauer. Oscillations and waves in a virally infected plankton system: Part I: The lysogenic stage. *Ecological Complexity*, 1(3):211–223, 2004.
- [30] Sarah Iams, Karna Gowda, and Mary Silber. Comparing reaction-diffusion models of vegetation patterns in semiarid ecosystems. In preparation.
- [31] Marten Scheffer, Stephen R Carpenter, Timothy M Lenton, Jordi Bascompte, William A Brock, Vasilis Dakos, Johan van de Koppel, I A van de Leemput, Simon A Levin, Egbert H van Nes, M Pascual, and J Vandermeer. Anticipating Critical Transitions. *Science*, 338(6105):344–348, October 2012.
- [32] Imanuel Noy-Meir. Desert ecosystems: environment and producers. *Annual review of ecology and systematics*, pages 25–51, 1973.
- [33] E Siero, Arjen Doelman, M B Eppinga, J D M Rademacher, M Rietkerk, and K Siteur. Striped pattern selection by advective reaction-diffusion systems: Resilience of banded vegetation on slopes. *Chaos: An Interdisciplinary Journal of Nonlinear Science*, 25(3):036411, March 2015.
- [34] Yuxin Chen, Theodore Kolokolnikov, Justin Tzou, and Chunyi Gai. Patterned vegetation, tipping points, and the rate of climate change. *European Journal of Applied Mathematics*, pages 1–14, June 2015.
- [35] S M Cox and P C Matthews. Exponential Time Differencing for Stiff Systems. *Journal of Computational Physics*, 176(2):430–455, March 2002.
- [36] Aly-Khan Kassam and Lloyd N Trefethen. Fourth-Order Time-Stepping for Stiff PDEs. *SIAM Journal on Scientific Computing*, 26(4):1214–1233, January 2005.
- [37] Aly-Khan Kassam. Solving reaction-diffusion equations 10 times faster. Technical report, University of Oxford, 2003.